

Formation and distribution of entrainment defects in gravity AISi7Cu0.5Mg alloy castings

G. Scampone, G. Timelli, R. Pirovano, S. Mascetti

In this study, the formation of entrainment defects in gravity permanent mould casting process was experimentally and numerically investigated. The distribution of oxide inclusions was mapped at the microscopic scale using metallographic and image analysis techniques. A fluid-dynamic simulation commercial software was used to predict the formation of defects and air entrapment during the casting process. The results showed that the typical casting defects detected throughout the castings were generated by the entrainment of bifilms. Moreover, the good agreement between the numerical results and the experimental findings proved that the numerical models had successfully predicted the entrainment phenomena, especially the formation of oxide inclusions and the entrapment of air bubbles.

KEYWORDS: ALUMINIUM ALLOYS, ENTRAINED AIR, BIFILM, MICROSTRUCTURE, NUMERICAL SIMULATION;

INTRODUCTION

The careful control of the casting process plays a key role in the final properties of aluminium (Al) alloy castings. The appropriately monitoring of the molten metal preparation, the pouring and the filling stages allow to produce high-performance components [1,2]. During these steps, due to the action of turbulence, the metal oxide surface can be easily entrained inside the liquid metal, resulting in filling defects called bifilms. These defects promote the formation of several solidification defects, such as gas and shrinkage porosity and hot tearing, which drastically decrease the performances of casting [2]. The use of numerical process simulation able to predict the damage caused by oxide inclusions can lead to the rapid optimisation of the process parameters and casting design, and to improve the final quality of the component.

In many papers from the literature, the characterization of oxide inclusions on the fracture surface and their impact on the mechanical properties have been investigated [3,4]. Other studies have correlated the numerical results of commercial simulation software with the experimental data related to the formation of macro-porosity

Giulia Scampone, Giulio Timelli

University of Padova, DTG, Italy

Raul Pirovano, Stefano Mascetti

XC Engineering Srl, Italy

[5]. However, to the best of the authors' knowledge, few works have been conducted to map the experimental distribution of entrainment defects at the microscopic scale and evaluate the severity of damage due to air and surface entrainment. This work aimed to compensate for this gap in the literature by studying the experimental and numerical distribution of oxide inclusions.

EXPERIMENTAL PROCEDURE

A primary AlSi7Cu0.5Mg cast alloy (EN AC-45500) was manually poured into a pre-heated permanent steel mould at 330 ± 3 °C. The pouring time and the molten metal temperature were 3 s and 735 ± 3 °C, respectively. The die,

shown in Figure 1, was made of AISI H11 tool steel and it allowed the casting of flat tensile test specimens with a rectangular cross-section of 10×6 mm². A 30-minute argon degassing treatment was conducted to improve the quality of molten metal and remove impurities and old oxides. Before each casting, the bath was manually skimmed with a coated paddle. No filtering operations, chemical eutectic modification or grain refinement were performed. During the experimental procedure, a batch of 6 castings was produced and 3 samples were separately poured for chemical composition analysis. Table 1 reports the average chemical composition of the alloy, measured by optical emission spectroscopy.

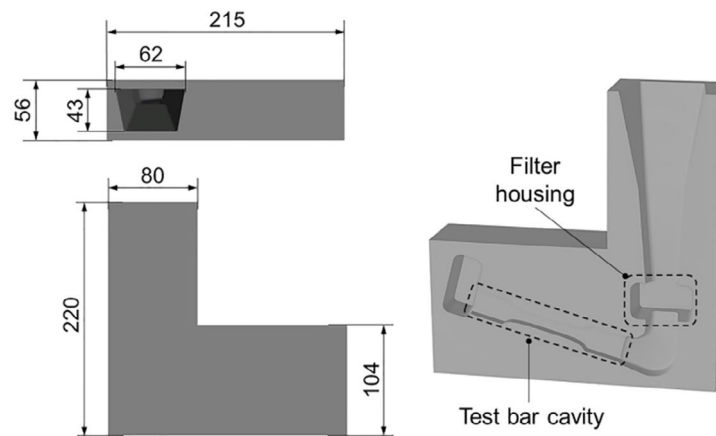


Fig.1 - Design of the permanent mould with overall dimensions (in mm).

Tab.1 - Chemical composition (wt.%) of the experimental AlSi7Cu0.5Mg alloy.

SI	FE	CU	MN	MG	NI	ZN	CR	TI	AL
6.50	0.089	0.652	0.012	0.431	0.005	0.004	0.014	0.121	bal.

The longitudinal section at half of the thickness of the tensile test specimen was selected for the metallographic investigation. The samples were drawn from each casting in correspondence of the filter zone and the test bar, and then they were mechanically prepared to a 3- μ m finish with diamond paste and polished with a commercial 0.04- μ m silica colloidal suspension.

An optical microscope was used to map the distribution of entrainment defects throughout the polished samples. Contiguous micrographs, each with an area of 1.2×0.9 mm², were automatically collected by exploiting the au-

tomatic handling of the microscope stage. To identify the oxide inclusions, a chemical etching was performed in a 5 vol% HF and 95 vol% H₂O solution.

Five severity grades (SGs) were identified to assess the severity of the oxide inclusions in the survey area. Each SG was defined according to the area of defects, which was quantitatively analysed using an image analyser. The area fraction covered by entrainment defects (A_D) was determined by dividing the total defect area measured in the micrograph by the entire area of the micrograph. Table 2 reports the different colours and ranges of A_D values as-

sociated with each SG. The A_D ranges were defined to emphasise low damage conditions. In general, SG equals to 1 corresponds to a region showing few closed bifilms or porosity with a maximum size of about 20 μm . The regions containing porosities with a maximum size of 300 μm and

coarser unfurled bifilms were classified as SG 4. The definition of these five SGs allowed to obtain a good resolution in the mapping of the casting damage.

Tab.2 - Ranges of area fraction covered by entrainment defects (A_D) used to assess the severity grades (SGs) caused by the entrainment of bifilms. For each SG, the associated colour is also reported.

Severity grade (SG)	Area fraction covered by entrainment defect	Associated colour
0	$A_D = 0\%$	
1	$0\% < A_D \leq 0.2\%$	
2	$0.2\% < A_D \leq 0.8\%$	
3	$0.8\% < A_D \leq 1.6\%$	
4	$1.6\% < A_D \leq 5\%$	

CASTING SIMULATION

The gravity die-casting workspace of FLOW-3D CAST v5.1 (2020) commercial software [6] was used to simulate the filling and solidification stages of the casting process. The three-dimensional (3D) computer-aided design model of the mould was imported into the simulation software. The physical properties of the die and the alloy were defined as linear functions of temperature within their respective operating temperature ranges. The process parameters were set using the empirical data collected during the experimental procedure. The gravity, adiabatic gas regions [7], $k-\omega$ turbulence [8] and surface tension [9] models were used during the casting simulation.

The air leakage from the two halves of the die was simulated by inserting virtual vents along the parting plane. Two probes were inserted at the beginning of the pouring channel to regulate the end of the pouring phase and avoid that the metal overflowed from the die.

A mesh of 747,000 cubic cells with a grid size of 1.5 mm was automatically generated by the software for the whole system (die and casting). The mesh was refined in correspondence with the interface between the mould halves, generating 572,000 cells for the die cavity.

The distribution of entrainment defects was numerically investigated by analysing the outputs of free surface defect concentration [10] and entrained air volume fraction [6].

RESULTS AND DISCUSSION

The typical casting defects detected throughout the microstructure were generated by the entrainment of bi-films. As shown in Figure 2, porosities were contoured by a thin oxide layer with a thickness in the range of 0.1 to 0.6 μm . The formation of solidification defects close to bifilms is consistent with many results reported in the literature [1-4]. As described by Campbell [2], the double oxide films acts like points for the growth of defects, because the unbounded oxide surfaces can be easily separated with minimal gas pressure or minimal stress, forming pores or cracks. The reduced film thickness here detected suggests that the formation of entrainment defects can be primarily associated to the pouring and filling stages. No thick oxides (i.e. old oxides) were observed, indicating the high quality of the metal before pouring and the efficiency of the degassing phase used in the present work.

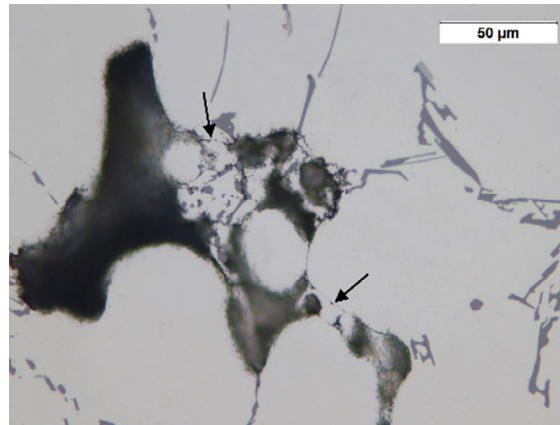


Fig.2 - A pore formed due to bifilm entrapment. The oxide layer contouring the pore is indicated by arrows.

Figure 3 shows the SG mapping related to oxide inclusions in the survey areas (filter zone and test bar). These two regions were hardly affected by entrapment defects: the average severity grade was lower than 0.8 (Table 3). The filter zone showed higher A_D values than the test bar, especially in the upper central area of the filter housing. The maximum SG value in the tensile stress test was equal to 2 and it was observed in 22 micro-graphs ($\sim 23.8 \text{ mm}^2$), while, in 74 fields ($\sim 79.9 \text{ mm}^2$) of the filter zone, the A_D values ranged between 0.2% and 5% ($\text{SG}=2+4$). This is in agreement with good foundry practice, where the mould design is optimized to avoid the accumulation of defects in the test bar [2].

In Table 3, a statistical analysis of the SG distribution is reported. About 60% of the investigated micrographs ($\sim 1783 \text{ mm}^2$) showed SG equal to 1, and 36.6% of the survey area was defect-free. Moreover, only 6 fields ($\sim 6.5 \text{ mm}^2$) had A_D higher than 0.8% ($\text{SG}=3$ or 4). The average SG in the test bar and the filter zone was equal to 0.6 and 0.8, respectively. These low values were related to the lack of old thick

oxides and a large number of small thin bifilms.

During the pouring and filling stages, the massive formation of young and fine bifilms may be caused by two main reasons: the height of the pouring channel and the short pouring time. The pouring height was about 210 mm, greater than 12.5 mm, which is the maximum height from which an Al alloy can fall without generating surface turbulence [2]. Tiryakioğlu et al. [10] proved that, due to the high kinetic energy of the metal flow that tears the surface oxide films, a filling velocity higher than 1 m/s increases the number density of porosities and reduces their size. In the current work, the filling velocity at the bottom of the sprue was higher than 1.5 m/s (Figure 4a), so during the impact with the die, the molten metal may have easily entrained oxide layers and bubbles, reducing its quality since the beginning of the casting. Moreover, the reduced pouring time (equal to 3 seconds) promoted high-speed flow and the generation of turbulence inside the die cavity.

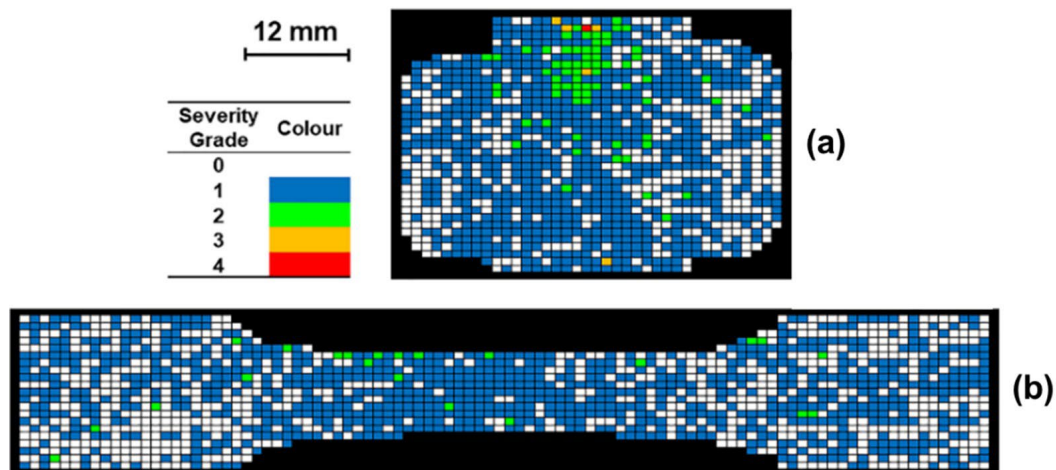


Fig.3 - Experimental distribution of the severity grade associated with entrapment defects (a) in the filter zone and (b) in the test bar.

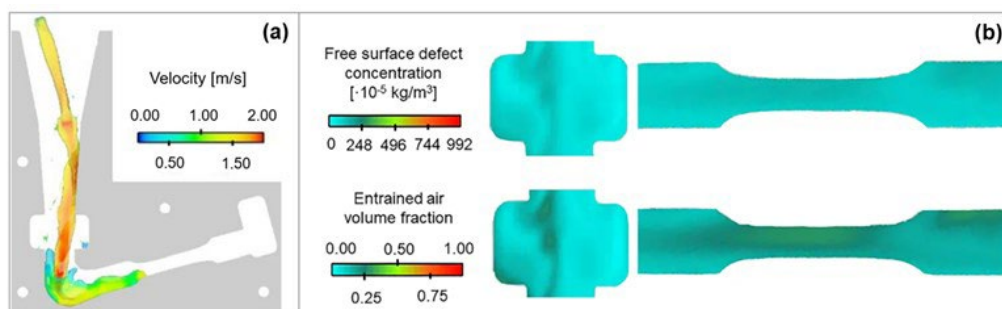
Tab.3 - Statistical analysis of the distribution of oxide related-defects. The number of fields for each SG was evaluated in the two survey areas.

Survey area	Severity grade					Mean
	0	1	2	3	4	
Filter zone	368	756	68	5	1	0.8
Test bar	639	895	22	0	0	0.6
Total number of fields	1007	1651	90	5	1	
Percentage on total	36.56%	59.95%	3.27%	0.18%	0.04%	

Figure 4b shows the numerical distribution of the free surface defect concentration and the entrained air volume fraction in the section at half the thickness of the tensile test specimen. The first parameter is mainly related to the formation of oxide inclusions that promote crack propagation, while the second output is more representative of bubble damage or gas porosity. Both these outputs were analysed to study the numerical distribution of defects generated by entrainment phenomena. The higher values of these two parameters were detected in the upper central area of the filter and in the gauge length of the tensile test bar, as shown in Figure 4b. These results were consistent

with the experimental findings and proved the reliability of the simulations performed.

It should be noted that the free-surface defect model, used to predict the formation of oxide inclusions, is based on some approximations in the modelling of the oxide film. In particular, the strength effect of the superficial oxide skin, the buoyancy of a bifilm, and its adhesion to the mould wall are not modelled [11]. However, in the current study, these approximations do not seriously affect the numerical distribution of oxide-related defects, as shown by the good agreement with the experimental results.

**Fig.4** - (a) Numerical distribution of filling velocity at 20 s from the beginning of the pouring. (b) Numerical outputs concerning the entrainment phenomena in the filter zone and the test bar at the end of the filling, when the liquid metal is at rest.

CONCLUSIONS

In the current work, the numerical and experimental distributions of entrainment defects in AlSi7Cu0.5Mg cast alloy were analysed. The experimental mapping of the severity grade related to entrainment phenomena was investigated, and the numerical outputs related to oxide for-

mation and air entrainment were studied. The following conclusions can be drawn.

- The generally low level of damage caused by entrainment defects is related to the molten metal velocity, higher than 1 m/s since the beginning of the filling. The high kinetic energy at the bottom of the

pouring basin promotes the tearing of the oxide film surface and the formation of a large number of reduced-in-size defects.

- The good agreement between the numerical results and the experimental findings indicates that the defect-prediction model has successfully predicted the entrainment phenomena, especially the entrapment of bubbles and oxide surfaces.

ACKNOWLEDGEMENTS

This research was developed with the financial support of Fondazione Cassa di Risparmio di Padova e Rovigo (CariPaRo). The Authors would like to thank Prof. M. Tiryakioğlu for the helpful tips and the stimulating reflections.

REFERENCES

- [1] Dispinar D., Campbell J. Effect of casting conditions on aluminium metal quality. *J. Mater. Process. Tech.* 2007; 182:405-410.
- [2] Campell J. *Complete Casting Handbook: Metal Casting Processes, Metallurgy, Techniques and Design.* Oxford-Waltham, MA: Butterworth-Heinemann; 2011. 11-13, 17-50, 67-72, 776, 833-852, 899-901 p.
- [3] Uludağ M., Çetin R., Dispinar D., Tiryakioğlu M. The effects of degassing, grain refinement & Sr-addition on melt quality-hot tear sensitivity relationships in cast A380 aluminum alloy. *Eng. Fail. Anal.* 2018; 90: 90-102.
- [4] El-Sayed M.A., Salem H.A., Kandeil A.Y. et al. Effect of Holding Time Before Solidification on Double-Oxide Film Defects and Mechanical Properties of Aluminum Alloys. *Metall. Mater. Trans. B* 2011; 42:1104-1109.
- [5] Cao H., Shen C., Wang C., Xu H., Zhu J. Direct Observation of Filling Process and Porosity Prediction in High Pressure Die Casting. *Materials.* 2019; 12:1099.
- [6] FLOW-3D® Version 12.0.2 Users Manual. 2020. FLOW-3D [Computer software]. Santa Fe, NM: Flow Science, Inc.
- [7] Hirt C.W., Barkhudarov M.R. Void Regions and Bubble Models in FLOW-3D. Flow Science Report 01-13. 2013; Flow Science, Inc., Santa Fe, NM.
- [8] Wilcox D.C. Formulation of the $k-\omega$ Turbulence Model Revisited. *AIAA Journal.* 2008; 46: 2823-2838.
- [9] Hirt C.W. Surface tension modeling. Flow Science Report 01-14, 2003; Flow Science, Inc., Santa Fe, NM.
- [10] Tiryakioğlu M., Yousefian P., Eason P.D. Quantification of Entrainment Damage in A356 Aluminum Alloy Castings. *Metall. Mater. Trans. A* 2018; 49:5815-5822.
- [11] Barkhudarov M.R., Hirt C.W. Tracking defects, in: 1st International Aluminium Casting Technology Symposium. 1998; Rosemont, IL.